

Twelve fundamental and two sextet fermion flavors

Zoltán Fodor

*Department of Physics, University of Wuppertal
Gaußstrasse 20, D-42119, Germany
Jülich Supercomputing Center, Forschungszentrum
Jülich, D-52425 Jülich, Germany
Email: fodor@bodri.elte.hu*

Kieran Holland

*Department of Physics, University of the Pacific
3601 Pacific Ave, Stockton CA 95211, USA
Email: kholland@pacific.edu*

Julius Kuti*

*Department of Physics 0319, University of California, San Diego
9500 Gilman Drive, La Jolla, CA 92093, USA
E-mail: jkuti@ucsd.edu*

Dániel Nógrádi

*Institute for Theoretical Physics, Eötvös University
H-1117 Budapest, Hungary
Email: nogradi@bodri.elte.hu*

Chris Schroeder*

*Physical Sciences Directorate, Lawrence Livermore National Laboratory
Livermore, California 94550, USA
E-mail: chris.schroeder@gmail.com*

Chik Him Wong

*Department of Physics 0319, University of California, San Diego
9500 Gilman Drive, La Jolla, CA 92093, USA
E-mail: rickywong@physics.ucsd.edu*

We report extended simulation results and their new analysis in two important gauge theories with twelve fermion flavors in the fundamental SU(3) color representation and two fermions in the sextet representation. We probe the $N_f = 12$ model with respect to the conformal window using mass deformed finite size scaling (FSS) theory driven by the fermion mass anomalous dimension. Our results at fixed gauge coupling show problems with the conformal scenario of the $N_f = 12$ model. In the sextet model with two flavors, under the conformal hypothesis, we determine large values for the anomalous fermion mass dimension with $\gamma \geq 1$. Since our sextet analysis favors the chiral symmetry breaking hypothesis without conformality, the large exponent γ could play an important role in understanding the composite Higgs mechanism. The new results discussed here include our extended data sets and exceed what was presented at the conference.

*The XXIX International Symposium on Lattice Field Theory - Lattice 2011
July 10-16, 2011, Squaw Valley, Lake Tahoe, California*

*Speaker.

1. Introduction

New physics at the Large Hadron Collider could be discovered in the form of some new strongly-interacting gauge theory with a composite Higgs mechanism, an idea which was outside experimental reach when it was first introduced as an attractive scenario beyond the Standard Model [1–9]. The original framework has been expanded by new explorations of the multi-dimensional theory space of nearly conformal gauge theories [10–18] where systematic and non-perturbative lattice studies play a very important role. Interesting models require the theory to be very close to, but below, the conformal window, with the gauge coupling slowly evolving over a large energy range. The non-perturbative knowledge of the critical number of flavors N_f^{crit} , separating the conformal phase from the phase of the composite Higgs mechanism with chiral symmetry breaking (χ SB), is essential and this has generated much interest with many old and new lattice studies [19–60]. The position of the conformal window with respect to the much discussed model of twelve fermions in the fundamental representation remains controversial with recent efforts from several lattice groups [19–34]. The position of the $N_f = 2$ sextet model with respect to the conformal window also remains unsettled [20, 44–48].

Probing the conformal and χ SB hypotheses we use two different strategies to deal with finite volume dependence. The first strategy extrapolates the spectrum to infinite volume at fixed fermion mass m where the leading finite size correction is exponentially small and determined by the lowest mass which has pion quantum numbers. From the mass spectrum of the infinite volume extrapolation we can probe the mass deformed conformal scaling behavior and compare with χ SB behavior when the fermion mass is varied in the infinite volume limit. The second strategy takes full advantage of the conformal FSS behavior without intrinsic scale when pressing against the $m = 0$ critical surface at fixed finite size L . Different from the first strategy, the finite volume corrections are not exponentially small and a much larger data set is analyzed closer to the critical surface. This is used in the $N_f = 12$ model, significantly extending our previously reported results [21]. We will also briefly summarize our main results in the sextet model where the first strategy is sufficient, since only runs at the lowest fermion mass show consistent and detectable finite volume dependence.

We have used the tree-level Symanzik-improved gauge action for all simulations in this paper. The conventional $\beta = 6/g^2$ lattice gauge coupling is defined as the overall factor in front of the well-known terms of the Symanzik lattice action. Its value is $\beta = 2.2$ for all simulations reported here for the $N_f = 12$ model. In the sextet model results are reported at $\beta = 3.2$. The link variables in the staggered fermion matrix were exponentially smeared with two stout steps [61]; the precise definition of the staggered stout action was given in [62]. The RHMC and HMC algorithms were deployed in all runs. For molecular dynamics time evolution we applied multiple time scales [63] and the Omelyan integrator [64]. Our error analysis of hadron masses used correlated fitting with double jackknife procedure on the covariance matrices. The time histories of the fermion condensate, the plaquette, and correlators are used to monitor autocorrelation times in the simulations.

2. Twelve fermion flavors in fundamental SU(3) color representation

Extending our earlier work [21], we have new simulation results at $\beta = 2.2$ in the fermion mass range $m = 0.002 - 0.025$ at lattice volumes $20^3 \times 40$, $24^3 \times 48$, $28^3 \times 56$, $40^3 \times 80$, and $48^3 \times 96$.

The extended data base now spans the $m = 0.002 - 0.035$ range. The new lowest fermion mass runs at $m = 0.002, 0.004, 0.006, 0.008$ can be used in the conformal FSS analysis which over the full set would correspond to a variation of the pion correlation length in the 2.5 to 20 range in the infinite volume limit. Results from the two lowest masses at $m = 0.002, 0.004$ are not included in the current analysis and will be reported later. For further control on finite volume dependence, large $48^3 \times 96$ runs were continued to two thousand trajectories at $m = 0.01$ and $m = 0.015$. Four runs were further added at $40^3 \times 80$ with $m = 0.01, 0.15, 0.02, 0.025$. The new and refreshed data set was subjected to conformal FSS analysis and χ SB tests of the $\langle \bar{\psi}\psi \rangle$ chiral condensate.

2.1 The phase diagram in the $\beta - m$ plane

The phase structure of the model remains controversial, particularly the critically important weak coupling phase. In addition to our spectroscopy and conformal FSS runs, we ran extensive scans at various fixed volumes and fixed fermion masses to explore the bulk phase structure. The bare coupling β was varied over a large range starting from very small β values deep in the strong coupling regime to the weak coupling phase at $\beta = 2.2$ where the conformal and χ SB analyses were done. Fermion masses $m = 0.007, 0.01, 0.02$ were used in the scans with spatial lattice sizes $L = 8, 12, 16, 20, 24, 32$ running a large densely spaced set in the important and much discussed intermediate region in transit from strong coupling to weak coupling. These scans were also extended to $N_f = 2, 4, 6, 8, 10, 12, 14, 16$ flavors. We will briefly summarize next what is known about the bulk lattice phase structure.

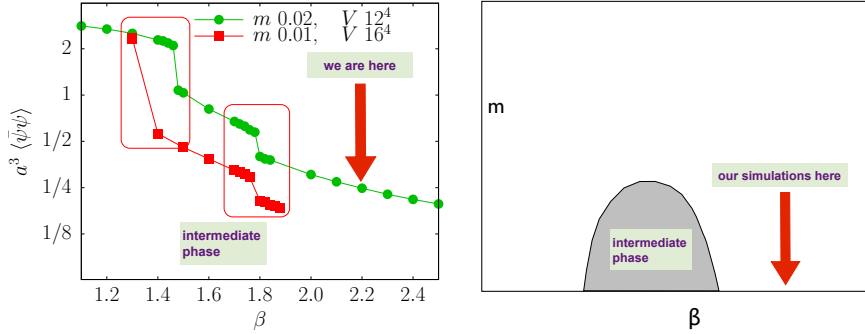


Figure 1: On the left, scans of the phase diagram by monitoring the chiral condensate are plotted as a function of β at two different fermion masses. The schematic bulk phase diagram is sketched on the right.

Two representative scans of the bulk behavior of the chiral condensate $\langle \bar{\psi}\psi \rangle$ are shown in Figure 1 as we vary β from strong to weak coupling. Three distinct regions emerge at fixed volume and fixed fermion mass showing strong coupling behavior for $\beta < 1.4$ with a large chiral condensate, an intermediate phase for $1.4 < \beta < 1.8$ with sudden drop in $\langle \bar{\psi}\psi \rangle$, and a weak coupling phase for $\beta > 1.8$ with further drop in $\langle \bar{\psi}\psi \rangle$. A similar structure of three regimes was also seen in scans at $N_f = 8$. Our physics simulations were done well inside the weak coupling phase at $\beta = 2.2$ as indicated in Figure 1. A similar structure has been observed independently by Deuzemen et al. [28] and Cheng et al. [31]. The newfound order parameter of broken shift symmetry in the intermediate phase is the most interesting development in the study of the esoteric intermediate phase [31]. It only exists in a finite interval of the lattice gauge coupling for small enough fermion masses, as

schematically sketched in Figure 1. The real interest is, of course, in the nature of the weak coupling phase. Based on axial U(1) symmetry considerations, arguments were presented in [28] in favor of conformal symmetry in the weak coupling phase. This argument was criticized and refuted in [31] based on new details of the broken shift symmetry with chiral symmetry restoration they discovered at zero temperature in the bulk intermediate phase.

Cheng et al. also presented their first weak coupling results on the Polyakov loop, the chiral condensate, and spectroscopy as indications of conformal symmetry in the weak coupling phase. The blocked Polyakov was reported to jump from zero to a large finite value in crossing to the weak coupling phase [31]. A confining potential was found in the intermediate phase with broken shift symmetry which turned into Coulomb potential without string tension in the weak coupling phase [31]. It was also noted that the observed chiral condensate and the related Dirac spectrum show the recovery of exact chiral symmetry in the massless fermion limit of the weak coupling phase consistent with observed degeneracies of parity partners even at finite fermion masses.

The results in [31] suggesting a chirally symmetric deconfined conformal phase are in contradiction with what we reported earlier [21] and further confirmed in the extended new analysis. Using lattice volumes several times larger we find a vanishing Polyakov loop at zero temperature in the weak coupling phase and a confining potential at a pion mass which is lower than in [31]. We also find the parity partners split at finite fermion mass. Our findings in large volumes are consistent with a chirally broken weak coupling phase. As a first step to resolve the contradictions, large finite volume effects acknowledged in [31] will have to be brought under better control.

In the next sub-sections we will briefly summarize our results on the chiral condensate, the finite temperature phase transition and tests of the conformal hypothesis in the weak coupling phase.

2.2 Chiral condensate and χ SB test

In the extended new analysis the chiral condensate (Fig. 2) remains consistent with χ SB in the massless fermion limit. Small changes in the fits are mostly driven by the two lowest fermion masses at $m = 0.01$ and $m = 0.015$ where runs on the largest $48^3 \times 96$ lattices were extended and new runs at higher masses on $40^3 \times 80$ lattices were added. A slight drift at the lowest $m = 0.01$ fermion mass was detected in the connected part of the condensate even after 1,400 trajectories (i.e., MD time units) and the run was continued to 2,000 trajectories. Since the finite volume analysis is incomplete, the largest volumes are used in the fitting range of the fermion masses. Finite volume extrapolations have to be completed before definitive conclusions can be drawn to establish a non-vanishing condensate $\langle \bar{\psi}\psi \rangle$ in the $m \rightarrow 0$ limit.

Details of the fitting procedure and the notation in Figure 2 were explained earlier [21]. The chiral condensate has a spectral representation [65] where the UV-divergent integral is written in a twice-subtracted form [66]. The UV contribution, which is divergent when the cutoff μa^{-1} is removed, has a linear term $\approx a^{-2} \cdot m$ and there is a third-order term $\approx m^3$ which is small and hard to detect for small m . The IR finite contributions to the chiral Lagrangian have a constant term $\approx BF^2$, a linear term $\approx B^2 \cdot m$, a quadratic term $\approx B^3 F^{-2} \cdot m^2$, and higher order terms, in addition to logarithmic corrections generated from chiral loops [67]. We kept a constant IR term and the linear and second order terms with UV and IR contributions. The second order fit in Figure 2 gives a non-vanishing condensate in the chiral limit which is roughly consistent with the GMOR [68] relation

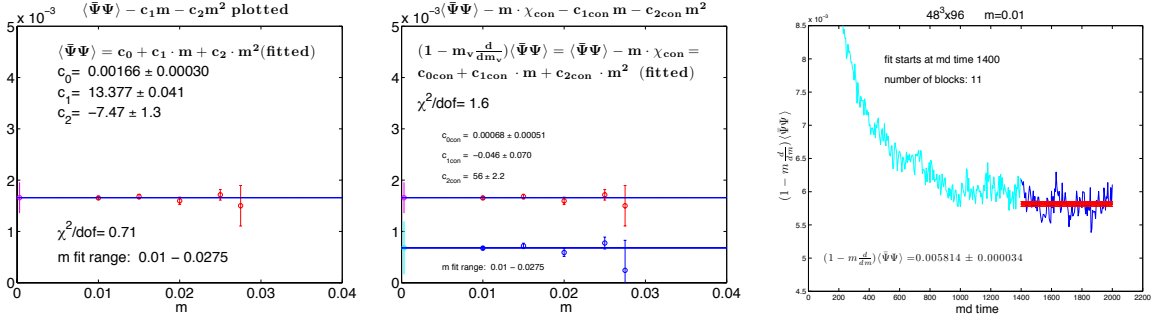


Figure 2: The second order polynomial fit to the chiral condensate is shown on the left plot in subtracted form as explained in [21]. The middle plot is the quadratic fit to $\langle \bar{\Psi}\Psi \rangle - m \cdot \chi_{con}$ directly measured from zero momentum sum rules and independently from functions of the inverse staggered fermion matrix. The right side plot shows the thermal history of the subtracted form of the condensate at the lowest fermion mass on the largest lattice.

$\langle \bar{\Psi}\Psi \rangle = 2F^2 B$ with the measured low value of F and the value of B from logarithmic fit to the Goldstone pion. The deficit between the two sides of the GMOR relation is sensitive to the fitting procedure and uncertainties in the determination of B . Trying to identify chiral logs is beyond the scope of our simulation range. For independent determination, we studied the subtracted chiral condensate operator defined with the help of the connected part χ_{con} of the chiral susceptibility χ as defined in [21]. The removal of the derivative term significantly reduces the dominant linear part of the $\langle \bar{\Psi}\Psi \rangle$ condensate. Although the two independent determinations give consistent non-vanishing results in the chiral limit, we cannot consider the results definitive. The drop of the chiral limit intercepts after extended runs is noted in comparison with earlier results [21].

2.3 Finite temperature transition

We present some preliminary results from our extended studies of the finite temperature transition. If the ground state of the model has χ_{SB} , a phase transition is expected at some finite temperature to restore the chiral symmetry in the limit of massless fermions. Based on universality arguments [69] the transition would be expected to be of first order. This is not entirely clear and warrants further investigations. On our largest $48^3 \times N_T$ lattices, at fixed $m = 0.01$ and $\beta = 2.2$, the temperature was varied through an N_T sequence while the scatter plot of the Polyakov loop was monitored along the euclidean time (inverse temperature) direction in each run. The chiral condensate $\langle \bar{\Psi}\Psi \rangle$ was also monitored in the runs. As the temperature is increased a clear sudden transition is observed in the $N_T = 6 - 10$ region where the Polyakov loop distribution jumps from the origin to a scatter plot with non-vanishing real part. It would be difficult to reconcile this jump, as shown in Figure 3, with conformal behavior in the zero temperature bulk phase.

Although we have results for temperature scans at multiple gauge couplings, fermion masses, and spatial volumes, all consistent with a finite temperature transition, caution is necessary before firm conclusions can be reached. Confirming the existence of the χ_{SB} phase transition will require the $m \rightarrow 0$ limits of $\langle \bar{\Psi}\Psi \rangle$ and the Polyakov loop distribution. The chiral condensate is a good order parameter for the transition. The Polyakov loop, like in QCD, could detect deconfinement in the transition with unsettled interpretation as order parameter. The behavior of the renormalized

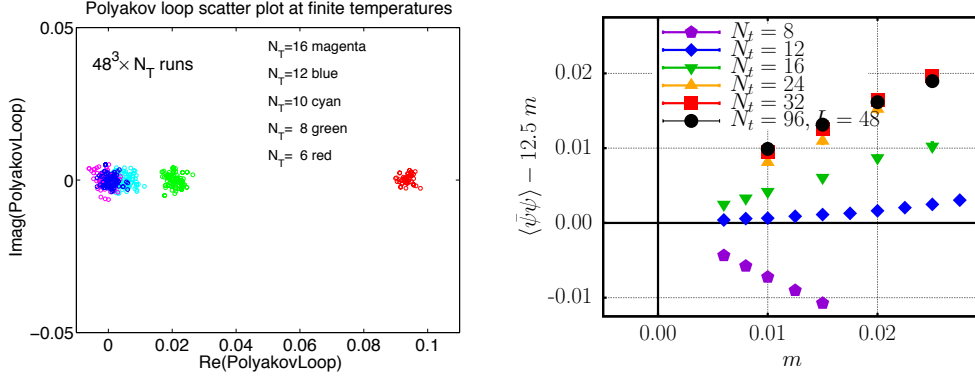


Figure 3: The scatter plot on the left side shows the Polyakov loop in the time direction as the temperature is varied using a sequence of lattice sizes $48^3 \times N_T$ at fixed $m = 0.01$ and $\beta = 2.2$ with N_T varied in the $N_T = 6, 8, 10, 12, 16$ range. On the right side plot the subtracted chiral condensate is plotted at $\beta = 2.2$ for a sequence of lattice sizes $48^3 \times N_T$ as the fermion mass is varied. The subtracted linear term $12.5 \cdot m$, chosen for the presentation of the data, is not determined from fits.

Polyakov loop is consistent with the scatter plot of Figure 3.

2.4 Conformal finite size scaling analysis

The expected leading FSS form for any mass M , or for F_π , scaled with the linear size L of the spatial volume, is given by a scaling function $L \cdot M = f(x)$ where $x = L \cdot m^{1/1+\gamma}$ is the conformal scaling variable. The scaling form sets in close to the critical surface for small m values. The scaling functions $f(x)$ can depend on the quantum numbers of the states but the scaling variable is expected to have the same form with identical γ exponent in each quantum number channel [39–42]. In sub-leading order there are conformal FSS scaling violation effects which are exhibited as a combined cutoff and L -dependent leading correction with the modified form $L \cdot M = f(x) + L^{-\omega} g(x)$ where the scaling correction exponent ω is determined at the infrared fixed point (IRFP) g^* of the β -function as $\omega = \beta'(g^*)$. This assumes that the mass deformation away from the critical surface is the only relevant perturbation around the IRFP. The leading scaling correction term close enough to the critical surface dominates any other corrections which are suppressed by further inverse powers of L . To detect the leading scaling violation effect requires high precision data with fits to scaling functions $f(x)$ and $g(x)$ and the critical exponent ω .

We applied conformal FSS theory to our data sets in the fermion mass range $m = 0.006 - 0.035$ with lattice sizes ranging in the fits from $20^3 \times 40$ to $48^3 \times 96$. Two different FSS fitting procedures were applied. In the first procedure, we defined a scaling function $f(x)$ for each mass M with five independent fitting parameters. The fitting function $f(x)$ was divided into two regions separated at the joint $x = x_{cut}$. Different forms were chosen on the two sides of x_{cut} from the expected conformal behavior. For large $x > x_{cut}$, the function $f(x) = c_1 x + c_{exp} (c_1 x)^{-1/2} \exp(-c_1 x)$ with parameters c_1 and c_{exp} describes the L -independent limit $M \sim c_1 m^{1/1+\gamma}$ at fixed m and $L \rightarrow \infty$. The c_{exp} amplitude sets the size of the leading small exponential correction from the finite volume effect of the lightest Goldstone pion state wrapping around the spatial volume. Since $f(0) = c_0$ is expected from conformal FSS with some power corrections at small x , we applied the simple

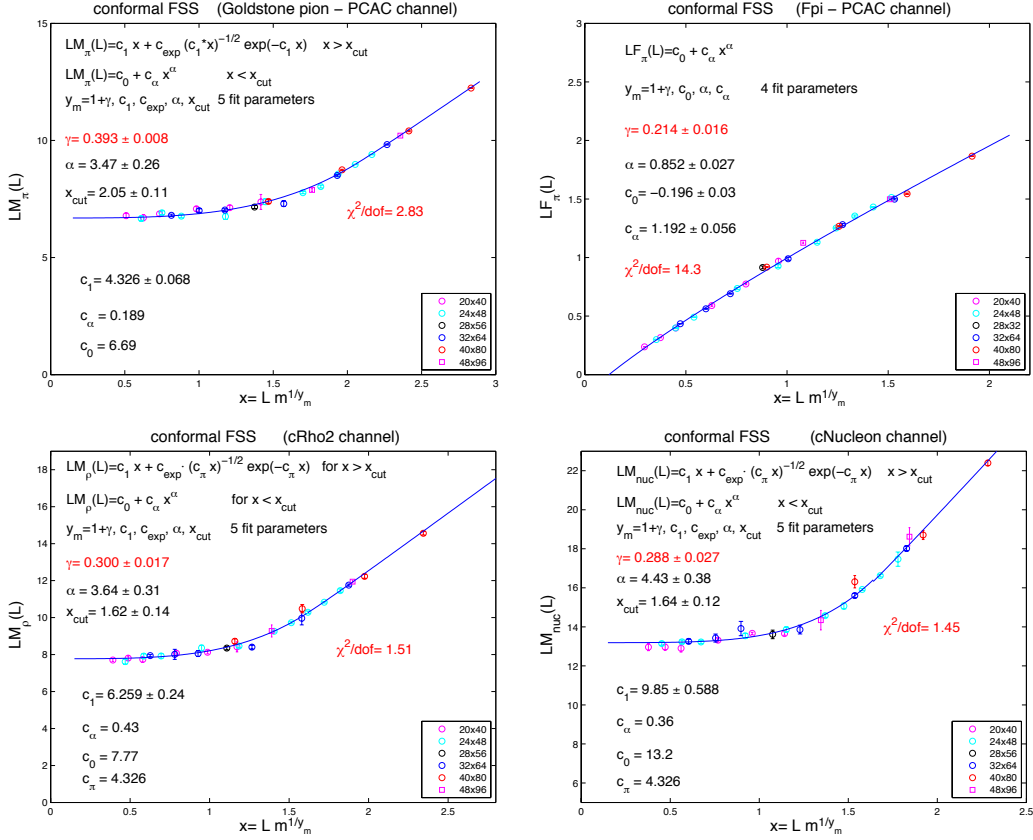


Figure 4: Conformal FSS fits in four different quantum number channels. The fits are performed in each channel separately. Since the γ values vary considerably from channel to channel, a simultaneous global fit to the combined channels with the same γ exponent, as required by conformal FSS theory, is bound to fail.

ansatz $f(x) = c_0 + c_\alpha x^\alpha$ for $x < x_{\text{cut}}$ (a more general polynomial function in the small x region is not expected to change the conclusions from the fits). From the fit to the PCAC Goldstone pion channel the parameter $c_\pi = c_1$ was determined and used as input in the exponential terms of the other channels with $\exp(-c_\pi L)$. The critical exponent γ was included among the five fitting parameters, in addition to c_0 , c_1 , c_{exp} , and x_{cut} .

The composite particle masses in several quantum number channels can be reasonably fitted with conformal scaling functions $f(x)$ as shown in Figure 4 but the values of the critical exponent γ are incompatible across different channels. The required global conformal FSS fit will fail with a single exponent γ across all quantum numbers. In the fits for F_π in the PCAC pion channel we only kept four parameters because the asymptotic form with exponentially small correction was zero within error. Actually, the data of F_π did not allow a successful conformal fit with any shape chosen for its scaling function $f(x)$ which looks very different from the scaling functions of composite particle masses. The unexpectedly curious LM_{nuc} behavior of the F_π data set against conformal FSS remains unresolved.

2.5 Generalized FSS fitting procedure with spline based general B-form

Following a new fitting strategy, we investigated if the failed global conformal FSS analysis can be attributed to restrictions on the conformal scaling functions $f(x)$. The restrictions were manifest in the physics-motivated fitting procedure we applied above. Our new general approach is different from [24, 45] but addresses related issues. We developed a general least-squares fitting procedure to the scaling functions using the B-form of spline functions without any further restrictions. In this procedure, the function $f(x)$ is described by piece-wise polynomial forms constructed from spline base functions with general coefficients in overlapping intervals of the scaling variable x . The shape of the B-form can be changed without limitations by increasing the number of base functions and the number of scaling intervals in x bracketing the overlapping data range. The details of this new analysis will be reported elsewhere [70].

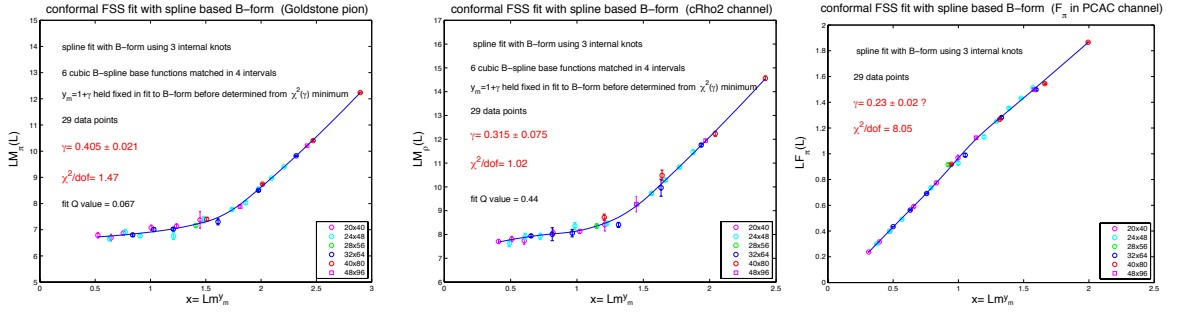


Figure 5: Conformal FSS fits using spline based B-forms in three different channels. The fits are preformed in each channel separately with the question mark on γ indicating difficulties of error estimates in bad fits of F_π .

Our fitting procedure in its setup requires two steps. In the first step, for any fixed choice of the exponent γ , the best fitted function $f(x)$ is determined in spline function B-form from the minimization of the weighted χ^2 expression. According to a general algorithm, the x -range of the data set is divided into intervals separated by internal knots and adding end point knots for B-form spline construction. The number of coefficients is determined by the number of knots and the order of the spline polynomials of the sub-intervals. The weighted χ^2 sum is minimized with respect to the coefficients of the base functions in the B-form. This will produce the best fit for fixed γ with a minimized χ^2 sum which will depend on γ . In the second step, we minimize the χ^2 sum with respect to γ to determine the best fit of the critical exponent. The one- σ confidence interval is determined from the variation of the χ^2 sum as a function of γ .

In Figure 5 we show three typical fits for illustration. The fit to the Goldstone pion in the PCAC channel improved as expected, with considerable increase in the error. The tension across channels decreased, as illustrated by comparison with the rho-channel fit, but the fit to F_π remained unacceptable. With the extended data set we are unable to reproduce results in [24, 45] which used tables from our earlier limited subset of data [21] in favor of consistency with the conformal phase. It is important to emphasize that we have not reached definitive conclusions about the failure of conformal tests. As we stated earlier [21], we have not analyzed yet the leading scaling violation effects and did not investigate if the good scaling form in separate quantum number channels can be explained in the chirally broken phase by strongly squeezed wave function effects. In disagreement

with [45], conformal FSS based analysis of the spectrum and related sum rules on moments of the correlators we have been developing are deep renormalization group based probes of the conformal phase. As explained in our forthcoming publication [70], we remain skeptical about the fitting procedure followed in [24] with efforts to rescue the conformal interpretation. The issues are not settled and ultimately will be decided in more definitive analyses.

3. Two fermion flavors in the sextet SU(3) color representation

This model has been studied recently by three BSM groups [20, 44, 46, 48]. Our findings are different from results based on the Schrödinger functional [44, 46] and compatible with the finite temperature phase transition in [48]. The disagreement with Schrödinger functional results is particularly significant based on the lower bound $\gamma \geq 1$ we find adopting the conformal hypothesis. This can be important in BSM applications and remains in contrast with the small exponent $\gamma < 0.45$ published in [46].

We have new simulation results at $\beta = 3.2$ in the fermion mass range $m = 0.003 - 0.010$ on $24^3 \times 48$ and $32^3 \times 64$ lattices. Five fermion masses at $m = 0.003, 0.004, 0.005, 0.006, 0.008$ are used in most fits. For further checks on finite volume dependence, a very large and expensive $48^3 \times 96$ run was added recently at $m = 0.003$ to follow the strategy of finite volume extrapolation at fixed fermion mass m . We also have new preliminary simulation results at $\beta = 3.25$ in the mass range $m = 0.004 - 0.008$ on $24^3 \times 48$ and $32^3 \times 64$ lattices. Based on the chiral and conformal analyses of the model, continued runs at existing run parameters and new runs are planned at both couplings to further probe the conformal FSS hypothesis in the sextet model following the strategy we presented for the $N_f = 12$ model.

3.1 Finite volume extrapolation

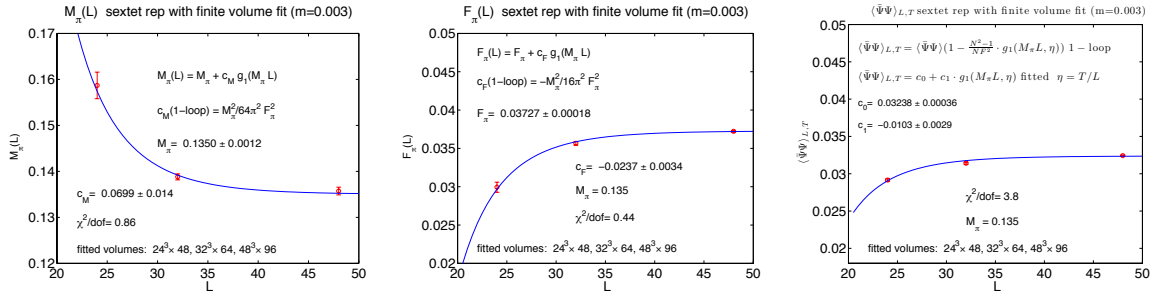


Figure 6: Finite volume dependence at the lowest fermion mass for $\beta = 3.2$. The form of $\tilde{g}_1(\lambda, \eta)$ is a complicated infinite sum which contains Bessel functions and requires numerical evaluation [71]. Since we are not in the chiral log regime, the prefactor of the $\tilde{g}_1(\lambda, \eta)$ function was replaced by a fitted coefficient. The leading term of the function $\tilde{g}_1(\lambda, \eta)$ is a special exponential Bessel function $K_1(\lambda)$ which dominates in the simulation range.

Based on the χ SB hypothesis, infinite volume extrapolations of the Goldstone pion, F_π , and $\langle \bar{\psi}\psi \rangle$ are shown in Figure 6 where $\tilde{g}_1(\lambda, \eta)$ describes the finite volume corrections with $\lambda = M_\pi \cdot L$ and aspect ratio $\eta = T/L$ from the lightest pion [72]. The fitting procedure approximates the leading treatment of the pion which wraps around the finite volume, whether in chiral perturbation

theory, or in Lüscher's non-perturbative finite volume analysis [73]. This does not require to reach the 1-loop chiral log limit as long as the pion is the lightest state dominating the finite volume corrections. The infinite volume limits of M_π , F_π , and $\langle\bar{\psi}\psi\rangle$ for $m = 0.003$ at $\beta = 3.2$ were determined self-consistently from the fitting procedure. Similar fits were applied to other composite states. Based on the fits at $m = 0.003$, one percent accuracy of the infinite volume limit is reached at $M_\pi L = 5$. In the fermion mass range $m \geq 0.004$ the condition $M_\pi L > 5$ is reached at $L = 32$. Although it will require high precision runs to test, we do not expect more than one percent residual volume dependence in the $32^3 \times 64$ runs for $m \geq 0.004$. Based on these observations, we will present chiral and conformal analyses with extrapolated infinite volume scaling behavior from the $32^3 \times 64$ runs for $m \geq 0.004$.

3.2 The chiral condensate and χSB

We follow the analysis of the chiral condensate as described for the $N_f = 12$ model. The $\langle\bar{\psi}\psi\rangle$ condensate data were fitted with a third order polynomial of the form $c_0 + c_1 m + c_2 m^3$ while the condensate with derivative subtraction was fitted without the linear term. Both independently measured quantities have to converge to the same chiral limit. The chiral condensate and its subtracted

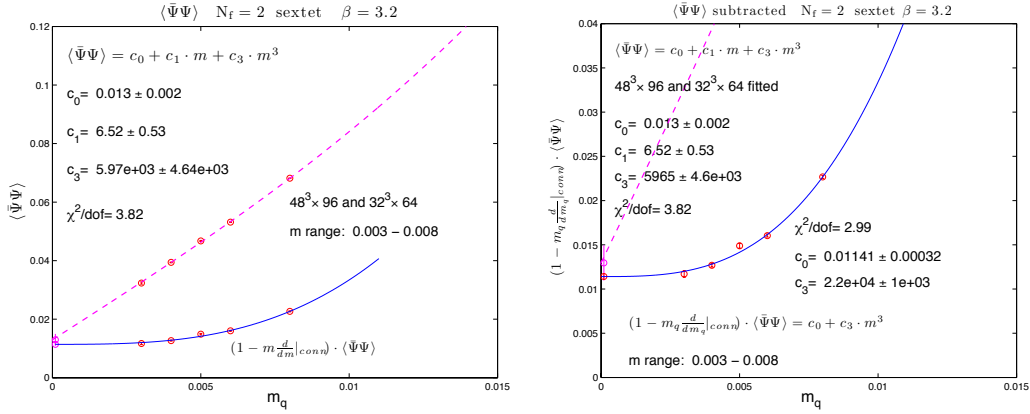


Figure 7: For any given $m \geq 0.004$ the largest volume condensate data is used since the finite volume analysis remains incomplete. The two plots are discussed in the text.

derivative version are shown in Figure 7 with a consistent strong χSB signal in the chiral limit.

3.3 Spectrum and the χSB hypothesis

Based on the analytic fermion mass dependence of the chiral Lagrangian, and using the lowest fermion masses in the $m = 0.003 - 0.008$ range, good polynomial fits were obtained without logarithmic loop corrections as shown in Figure 8 for four select states. The plotted $24^3 \times 48$ data points for $m \geq 0.004$ agree with the fitted data from the $32^3 \times 64$ runs indicating the infinite volume limit within the accuracy of the data. Small corrections, if required, should not effect the conclusions. Although we could fit M_π and F_π with the continuum chiral logarithms included, the separate sets of F and B from the fits are not quite self-consistent. A combined staggered SU(2) chiral perturbation theory fit is required for simultaneous fits of M_π and F_π with a consistent pair of fundamental chiral parameters F and B . The explicit cutoff dependent corrections to the F and B parameters

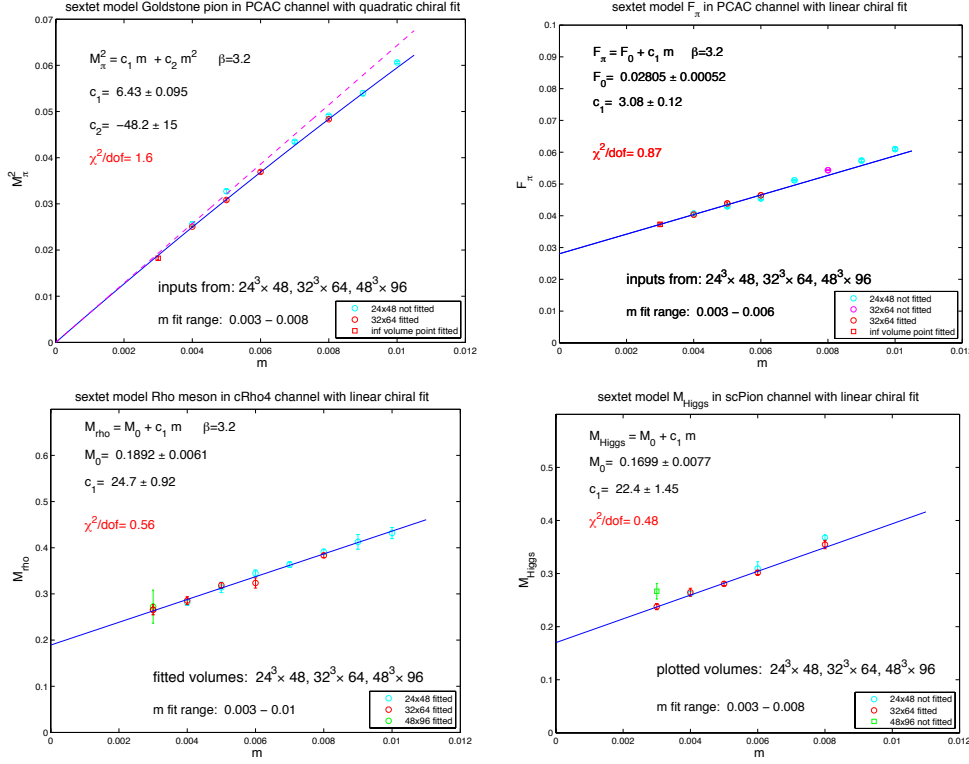


Figure 8: Polynomial fits from the analytic mass dependence of the chiral Lagrangian without logarithmic loop corrections are shown for the Goldstone pion, F_π , M_ρ , and the 0^{++} state with mass M_{Higgs} . The dashed line in the Goldstone pion plot shows the leading linear contribution. F_0 on the top right plot sets the electroweak vev scale. The disconnected diagram, which can shift the final value of the Higgs mass from $M_0 = 6.06 \cdot F_0$ on the bottom right plot, is not included in the calculation.

would require further testing at weaker gauge couplings and using partially quenched staggered chiral perturbation theory. Our runs at $\beta = 3.25$ should provide the data for this analysis.

3.4 Conformal hypothesis and the critical exponent γ

It is important to compare the polynomial fits with conformal scaling behavior for small mass deformations m . In the infinite volume limit the masses of composite particles and F_π are expected to scale as $M \sim m^{1/\gamma}$ with the same exponent γ in all channels. When the four lowest fermion mass values closest to the critical surface are fitted separately with the leading conformal form, we get good χ^2 fits but very different γ exponents, which is not consistent with mass deformed conformal behavior. The conflicting fits are illustrated side by side in Figure 9 for the Goldstone pion and the F_π decay constant. Fitting to the pion mass requires $\gamma = 1.091(34)$ while the F_π fit is forcing $\gamma = 2.13(18)$. In the combined fit they compromise with $\gamma = 1.47(26)$ and the unacceptable $\chi^2/\text{dof} = 31.1$. It is very difficult to see how this conflict, also in disagreement with [46], could be resolved within the conformal hypothesis. From the tests we were able to perform, the sextet model is consistent with χSB and inconsistent with conformal symmetry. It will require further investigations to show that subleading effects cannot alter this conclusion. We will consider com-

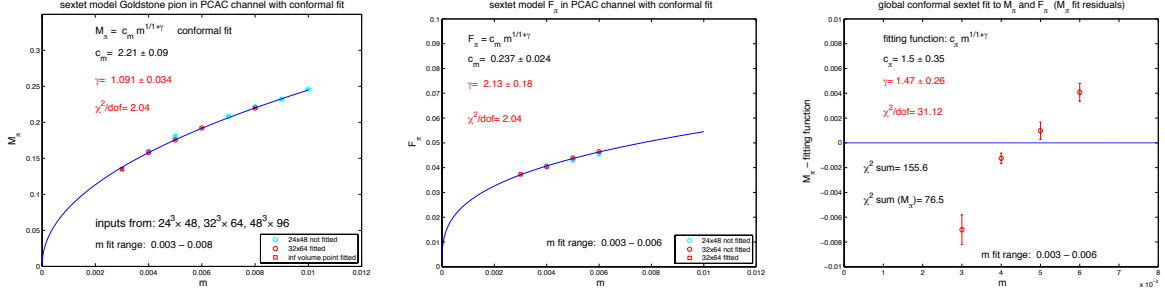


Figure 9: The left side plot and the middle plot represent separate conformal fits. The right side plot display the M_π residuals from the global fit. It is unacceptable for F_π as well. The global fit is trying to choose a γ value between $\gamma \sim 1$ in the Goldstone pion channel and $\gamma \sim 2$ in the F_π fit resulting in a very high χ^2 value. All fits are at $\beta = 3.2$.

prehensive conformal FSS tests which do not rely on infinite volume extrapolation in the scaling fits. This is at a preliminary stage requiring new runs and systematic analysis.

If χSB of the sextet model is further confirmed in the massless fermion limit, its relevance for the realization of the composite Higgs mechanism is transparent. The large anomalous exponent γ of our conformal fits will be interpreted in this case as an important ingredient of the model in the χSB phase. Importantly, the model has the perfect match of three Goldstone pions to provide the longitudinal components of the W^\pm and Z bosons. To understand the slowly changing gauge coupling close to the conformal window without infrared fixed point will require high precision methods to calculate the renormalized gauge coupling and its beta function. This will demand extended and more reliable Schrödinger functional analysis or alternate methods which are being developed. The difference between the large exponent γ reported here and the low value of γ published earlier [46] is significant and will require clarifications. Conformal FSS tests very close to the critical surface will provide further independent checks of our results.

Acknowledgments

We are grateful to Kalman Szabo and Sandor Katz for their code development and to Anna Hasenfratz for discussions. The simulations were performed using computational resources at Fermilab and JLab, under the auspices of USQCD and SciDAC. This research is supported by the NSF under grants 0704171 and 0970137, by the DOE under grants DOE-FG03-97ER40546, DOE-FG-02-97ER25308, by the DFG under grant FO 502/1 and by SFB-TR/55, and the EU Framework Programme 7 grant (FP7/2007-2013)/ERC No 208740. Some of the simulations used allocations from the Extreme Science and Engineering Discovery Environment (XSEDE), which is supported by National Science Foundation grant number OCI-1053575.

References

- [1] S. Weinberg, Phys. Rev. D **19**, 1277 (1979).
- [2] L. Susskind, Phys. Rev. D **20**, 2619 (1979).
- [3] S. Dimopoulos, L. Susskind, Nucl. Phys. **B155**, 237-252 (1979).

- [4] E. Eichten, K. D. Lane, Phys. Lett. **B90**, 125-130 (1980).
- [5] E. Farhi and L. Susskind, Phys. Rept. **74**, 277 (1981).
- [6] B. Holdom, Phys. Lett. **B150**, 301 (1985).
- [7] K. Yamawaki, M. Bando, K. -i. Matumoto, Phys. Rev. Lett. **56**, 1335 (1986).
- [8] T. Appelquist, L. C. R. Wijewardhana, Phys. Rev. **D36**, 568 (1987).
- [9] V. A. Miransky and K. Yamawaki, Phys. Rev. D **55**, 5051 (1997).
- [10] W. E. Caswell, Phys. Rev. Lett. **33**, 244 (1974).
- [11] T. Banks and A. Zaks, Nucl. Phys. B **196**, 189 (1982).
- [12] T. Appelquist, M. Piai, R. Shrock, Phys. Rev. **D69**, 015002 (2004).
- [13] F. Sannino, K. Tuominen, Phys. Rev. **D71**, 051901 (2005).
- [14] D. D. Dietrich, F. Sannino, K. Tuominen, Phys. Rev. **D72**, 055001 (2005).
- [15] M. A. Luty, T. Okui, JHEP **0609**, 070 (2006).
- [16] D. D. Dietrich, F. Sannino, Phys. Rev. **D75**, 085018 (2007).
- [17] M. Kurachi, R. Shrock, JHEP **0612**, 034 (2006).
- [18] M. Mojaza, C. Pica, F. Sannino, Phys. Rev. **D82**, 116009 (2010).
- [19] Z. Fodor, K. Holland, J. Kuti, D. Negradi and C. Schroeder, Phys. Lett. B **681**, 353 (2009).
- [20] Z. Fodor, K. Holland, J. Kuti, D. Negradi and C. Schroeder, arXiv:1103.5998 [hep-lat].
- [21] Z. Fodor, K. Holland, J. Kuti, D. Negradi, C. Schroeder, Phys. Lett. B **703**, 348 (2011) [arXiv:1104.3124 [hep-lat]].
- [22] T. Appelquist, G. T. Fleming and E. T. Neil, Phys. Rev. Lett. **100**, 171607 (2008).
- [23] T. Appelquist, G. T. Fleming and E. T. Neil, Phys. Rev. D **79**, 076010 (2009),
- [24] T. Appelquist, G. T. Fleming, M. F. Lin, E. T. Neil and D. A. Schaich, Phys. Rev. D **84**, 054501 (2011) [arXiv:1106.2148 [hep-lat]].
- [25] T. Appelquist *et al.*, Phys. Rev. Lett. **104**, 071601 (2010).
- [26] A. Deuzeman, M. P. Lombardo, E. Pallante, Phys. Lett. **B670**, 41-48 (2008).
- [27] A. Deuzeman, M. P. Lombardo, E. Pallante, Phys. Rev. **D82**, 074503 (2010).
- [28] A. Deuzeman, M. P. Lombardo, T. N. da Silva and E. Pallante, arXiv:1111.2590 [hep-lat].
- [29] A. Hasenfratz, Phys. Rev. **D80**, 034505 (2009).
- [30] A. Hasenfratz, Phys. Rev. **D82**, 014506 (2010).
- [31] A. Cheng, A. Hasenfratz and D. Schaich, arXiv:1111.2317 [hep-lat].
- [32] X. -Y. Jin, R. D. Mawhinney, PoS **LAT2009**, 049 (2009).
- [33] X. -Y. Jin, R. D. Mawhinney, PoS **LATTICE2010**, 055 (2010).
- [34] Y. Aoki, T. Aoyama, M. Kurachi, T. Maskawa, K. -i. Nagai, H. Ohki, A. Shibata and K. Yamawaki *et al.*, arXiv:1202.4916 [hep-lat].
- [35] S. Catterall, F. Sannino, Phys. Rev. **D76**, 034504 (2007).
- [36] S. Catterall, J. Giedt, F. Sannino, J. Schneible, JHEP **0811**, 009 (2008).
- [37] A. J. Hietanen, J. Rantaharju, K. Rummukainen, K. Tuominen, JHEP **0905**, 025 (2009).

- [38] A. J. Hietanen, K. Rummukainen, K. Tuominen, Phys. Rev. **D80**, 094504 (2009).
- [39] L. Del Debbio, B. Lucini, A. Patella, C. Pica, A. Rago, Phys. Rev. **D82**, 014510 (2010).
- [40] F. Bursa, L. Del Debbio, L. Keegan, C. Pica, T. Pickup, Phys. Lett. **B696**, 374-379 (2011).
- [41] L. Del Debbio, R. Zwicky, Phys. Rev. **D82**, 014502 (2010).
- [42] L. Del Debbio, B. Lucini, A. Patella, C. Pica and A. Rago, arXiv:1111.4672 [hep-lat].
- [43] Y. Shamir, B. Svetitsky, T. DeGrand, Phys. Rev. **D78**, 031502 (2008).
- [44] T. DeGrand, Y. Shamir, B. Svetitsky, Phys. Rev. **D82**, 054503 (2010).
- [45] T. DeGrand, Phys. Rev. D **84**, 116901 (2011) [arXiv:1109.1237 [hep-lat]].
- [46] T. DeGrand, Y. Shamir and B. Svetitsky, arXiv:1201.0935 [hep-lat].
- [47] J. B. Kogut, D. K. Sinclair, Phys. Rev. **D81**, 114507 (2010).
- [48] D. K. Sinclair, J. B. Kogut, PoS **LATTICE2010**, 071 (2010).
- [49] E. Bilgici, A. Flachi, E. Itou, M. Kurachi, C. -J D. Lin, H. Matsufuru, H. Ohki, T. Onogi *et al.*, Phys. Rev. **D80**, 034507 (2009).
- [50] E. Itou, T. Aoyama, M. Kurachi, C. -J. D. Lin, H. Matsufuru, H. Ohki, T. Onogi, E. Shintani *et al.*, PoS **LATTICE2010**, 054 (2010).
- [51] N. Yamada, M. Hayakawa, K. -I. Ishikawa, Y. Osaki, S. Takeda, S. Uno, PoS **LAT2009**, 066 (2009).
- [52] M. Hayakawa, K. -I. Ishikawa, Y. Osaki, S. Takeda, S. Uno, N. Yamada, [arXiv:1011.2577 [hep-lat]].
- [53] R. V. Gavai, Nucl. Phys. **B269**, 530 (1986).
- [54] N. Attig, B. Petersson, M. Wolff, Phys. Lett. **B190**, 143 (1987).
- [55] J. B. Kogut, D. K. Sinclair, Nucl. Phys. **B295**, 465 (1988).
- [56] S. Meyer, B. Pendleton, Phys. Lett. **B241**, 397-402 (1990).
- [57] P. H. Damgaard, U. M. Heller, A. Krasnitz, P. Olesen, Phys. Lett. **B400**, 169-175 (1997).
- [58] S. -y. Kim, S. Ohta, Phys. Rev. **D46**, 3607-3617 (1992).
- [59] F. R. Brown, H. Chen, N. H. Christ, Z. Dong, R. D. Mawhinney, W. Schaffer, A. Vaccarino, Phys. Rev. **D46**, 5655-5670 (1992).
- [60] Y. Iwasaki, K. Kanaya, S. Kaya, S. Sakai, T. Yoshie, Phys. Rev. **D69**, 014507 (2004).
- [61] C. Morningstar and M. J. Peardon, Phys. Rev. D **69**, 054501 (2004).
- [62] Y. Aoki, Z. Fodor, S. D. Katz, K. K. Szabo, JHEP **0601**, 089 (2006).
- [63] C. Urbach, K. Jansen, A. Shindler, U. Wenger, Comput. Phys. Commun. **174**, 87-98 (2006).
- [64] T. Takaishi, P. de Forcrand, Phys. Rev. **E73**, 036706 (2006).
- [65] T. Banks and A. Casher, Nucl. Phys. B **169**, 103 (1980).
- [66] H. Leutwyler, A. V. Smilga, Phys. Rev. **D46**, 5607-5632 (1992).
- [67] J. Bijnens, J. Lu, JHEP **0911**, 116 (2009). [arXiv:0910.5424 [hep-ph]].
- [68] M. Gell-Mann, R. J. Oakes and B. Renner, Phys. Rev. **175**, 2195 (1968).
- [69] R. D. Pisarski, F. Wilczek, Phys. Rev. **D29**, 338-341 (1984).
- [70] Z. Fodor, K. Holland, J. Kuti, D. Negradi, C. Schroeder, C. H. Wong, *in preparation*.
- [71] J. Gasser, H. Leutwyler, Phys. Lett. **B184**, 83 (1987).
- [72] H. Leutwyler, Phys. Lett. B **189**, 197 (1987).
- [73] M. Luscher, Commun. Math. Phys. **104**, 177 (1986).